



OPEN Optimization of the single-side drift method for shallow-buried tunnels under large eccentric pressure based on the BiDoseResp settlement model

Ruijie Sun^{1,2}, Bin Gao², Chuan Gan¹✉, Jian Zhu¹, Dongming Cai¹ & Lingbing Yi²

Taking a twin-tunnel project in Qinghai Province as a case study, this research investigates the excessive vault settlement of 14.8 cm observed at the right portal section. A three-dimensional finite element model was established to simulate the complete construction process using the single-side drift method. The results indicate that the “removal of the middle partition wall” acts as the critical factor triggering abrupt settlement. Innovatively, the BiDoseResp dual-dose response function was introduced, achieving high-precision fitting of the entire settlement–time history ($R^2 = 0.9957$). Using the validated model, two excavation sequences—shallow-buried side first versus deep-buried side first—were compared. Excavating from the deep-buried side first (Scheme B) reduced vault settlement on the shallow-buried side by 18.4%–20.5% and decreased the maximum axial forces in the support structure by up to 55.9%. Based on these findings, a risk control strategy was proposed for the left portal section, which prioritizes excavation from the deep-buried side, minimizes the exposure time of the middle partition wall, and incorporates dynamic settlement prediction via the BiDoseResp model. The outcomes offer theoretical insights and technical solutions for informatized construction and deformation early-warning in shallow-buried tunnels subjected to large bias pressures.

Keywords Shallow-buried tunnel under large bias pressure, Single-side drift method, BiDoseResp model, Vault settlement, Excavation sequence optimization

The portal section of shallow-buried tunnels under large asymmetrical pressure represents a high-risk zone in mountain tunnel construction. Characteristics such as shallow depth, significant topographic inclination, and weathered, fragmented surrounding rock mass render these sections prone to issues including excessive vault settlement, surface cracking, and even structural instability. Consequently, deformation control and stability assurance have remained persistent research foci in tunnel engineering^{1,2}. Due to the coupling effect of asymmetrical loading and shallow burial conditions, the stress distribution within the surrounding rock is highly non-uniform. Furthermore, the supporting structure must simultaneously withstand both asymmetric loads and excavation-induced disturbances, resulting in a construction complexity substantially greater than that of conventional tunnels.

Current research on shallow-buried tunnels under large asymmetrical pressure has achieved notable progress. Regarding deformation mechanisms, scholars have utilized field monitoring and numerical simulations to elucidate the evolution of tunnel displacement throughout the construction sequence of methods such as the single-side drift method. These studies have confirmed the substantial influence of key procedures, including excavation sequence and the removal of temporary support, on deformation control. For instance, Pan et al.³ applied the direct boundary element method to investigate the stress characteristics of shallow-buried tunnels under both non-uniform surface traction and symmetric gravity loads, concluding that eccentric loads significantly alter the stress regime in the surrounding rock mass. Liu⁴ and Yang et al.⁵ focused on the characteristics of displacement variation under different excavation sequences. Sharifzadeh et al.⁶ evaluated the stability of surrounding rock under six different excavation sequences using a three-dimensional finite element

¹Key Laboratory of Urban Security and Disaster Engineering, Ministry of Education, Beijing University of Technology, Beijing 100124, China. ²China Communications Construction Railway Transportation Division (Railway Transportation Branch/Railway General Research Institute), Beijing 100088, China. ✉email: 1004336127@qq.com

model. Li et al.⁷ proposed that excavating the tunnel's upper bench first can expedite construction progress and is beneficial for maintaining an appropriate offset distance between tunnel faces. Furthermore, Chen et al.⁸ analyzed the failure mechanism of the Muzhailing Tunnel and summarized the key characteristics of large deformations from six perspectives: failure mode, groundwater influence, sensitivity of influencing factors, magnitude of deformation, deformation rate, and deformation duration.

In the realm of risk control for tunnel construction, advanced support techniques—such as large pipe roofs and small conduits—along with the optimization of initial support parameters, have emerged as critical technical measures to effectively mitigate collapse risks during construction. Carranza-Torres et al.⁹ conducted analyses on composite tunnel linings, while Das and Xiao investigated the behavior of tunnel supports under asymmetric loading conditions^{10,11}. Tang et al.¹² examined stress variations in the surrounding rock and support system following the excavation of a large-span shallow-buried tunnel under asymmetrical pressure, thereby establishing a rational excavation scheme. Through on-site monitoring of a tunnel subject to asymmetrical loading, Wang et al.¹³ analyzed contributing factors such as rainwater infiltration, low rock strength, and biased ground stress. They implemented reinforcement measures—including temporary steel arches, vertical supports, diagonal bracing, and temporary invert arches—to curb the progression of large deformations. Lei et al.¹⁴ used numerical simulation to determine the stress state of tunnels under varying surface slopes, and in another study¹⁵, analyzed the failure mechanism and load characteristics of surrounding rock in a shallow-buried biased tunnel with a small clear spacing. Habumuremyi et al.¹⁶ examined the stability of shield tunnel faces, while Amiri et al.¹⁷ and Mojtahedi et al.¹⁸ respectively discussed tunnel stability under different construction methods and in varying rock mass conditions. Zhang et al.¹⁹ developed a three-dimensional discrete element model of a twin-arch tunnel under inclined asymmetric stresses, analyzing the effects of joint dip angle and spacing on deformation, the evolution of bedding-induced asymmetric stresses, and the stability of the middle partition wall. They proposed an optimized excavation and support scheme to achieve a nearly balanced stress distribution (ratio ≈ 1) on both sides of the tunnel under equivalent overburden depth. Focusing on a shallow-buried large-span tunnel under biased pressure, Chen et al.²⁰ used FLAC3D to compare three excavation methods: the Tunnel Excavation Method (TEM), the Center Diaphragm Method (CDM), and the Double Side Drift Method (DSDM). Their results verified that the DSDM offers superior control of surrounding rock deformation and improved slope stability. In a case study of a super-large cross-section highway tunnel, Huang et al.²¹ combined field monitoring with ABAQUS simulations to compare the double-side drift, CRD, and three-bench seven-step excavation methods. They demonstrated that the double-side drift method minimizes deformation in both the surrounding rock and support structure, provided that initial support is installed promptly to alleviate stress concentration. Feng et al.²² applied the Simplified Rigid Upper Bound Limit Analysis Method (RBUBM) to study failure mechanisms and surface settlement in inclined strata. Their results indicated that the ultimate support pressure fluctuates within $\pm 21\%$ – 25% , with the settlement zone shifting as the dip angle changes. A fitting formula for surface settlement was proposed, offering a valuable reference for the design of tunnels in inclined ground. To predict shield-induced surface settlement, Zhao et al.²³ introduced an improved Informer algorithm, which substantially reduced the time required for computational forecasting.

In shallow-buried tunnels subjected to significant asymmetric pressure, a complex coupling mechanism exists between the deformation behavior of weathered rock masses and the dynamic response of support structures. On the one hand, weathered slate exhibits marked nonlinear deformation and time-dependent effects following excavation and unloading. Its strength degradation, crack propagation, and creep behavior directly govern the stress evolution in the supporting elements. On the other hand, the stiffness, installation timing, and removal sequence of support members—such as shotcrete layers, steel arches, and the middle partition wall—reciprocally influence the surrounding rock, collectively forming a synergistic rock–support interaction system. This coupling mechanism becomes particularly pronounced in the single-side drift method. During the removal of the middle partition wall, for instance, an abrupt reduction in support stiffness can trigger a rapid stress redistribution in the surrounding rock, leading to a stepped increase in crown settlement.

A number of researchers have examined this rock–support interaction from various perspectives. He et al.²⁴, for example, investigated the mechanical response and construction optimization of a shallow-buried, super-large-span tunnel in weathered tuff strata. They proposed an optimized construction procedure and numerically validated that construction disturbances are concentrated during the upper bench excavation, with the excavation of the upper bench of the middle pilot tunnel representing the most critical stage. Their results also indicated that blasting vibrations in the middle pilot tunnel can induce damage to temporary supports. Hu et al.²⁵ combined physical model tests with FLAC3D numerical simulations to analyze the mechanical behavior of both the surrounding rock and support system in a shallow-buried biased tunnel traversing a soil–rock interface. Similarly, Sun et al.²⁶ integrated block theory tests with UDEC numerical simulations to study displacement patterns and failure mechanisms in a shallow-buried jointed rock tunnel under tectonic stresses.

However, current research still exhibits notable limitations. First, most studies focus primarily on the influence of individual factors—such as the excavation method or support parameters—on tunnel stability, while lacking a systematic investigation into the coupling mechanism between the inherent deformation characteristics of weathered rock masses and the dynamic response of support structures. Second, conventional settlement prediction models struggle to accurately capture the nonlinear deformation features arising from the multi-stage superposition of “excavation disturbance–temporary support removal–surrounding rock creep” under asymmetrical pressure conditions. Consequently, these models exhibit insufficient predictive accuracy for deformation mutations occurring at key construction stages, such as during the removal of the middle partition wall.

To address these gaps, this study systematically investigates a twin-tunnel project in Qinghai Province characterized by shallow burial and large asymmetrical pressure. Focusing on the excessive vault settlement observed at the right portal section, we integrate field monitoring, three-dimensional numerical simulation, and

| Support name | Size/cm | Profile |
|------------------------------|---------------------------|--------------------------------------|
| Initial support | 26 | C25 shotcrete |
| System anchor bolt | 350 | Hollow bolt with a diameter of 25 mm |
| Advanced small pipe | 450 | A42 × 4 mm grouting small pipe |
| Large pipe shed | 3000 | A108 × 8 steel pipe |
| Temporary support steel arch | 60 (longitudinal spacing) | I16 steel arch |
| Internal partition wall | 18 | C25 shotcrete |
| Secondary lining | 50 | C35 reinforced concrete |

Table 1. Tunnel support parameters.

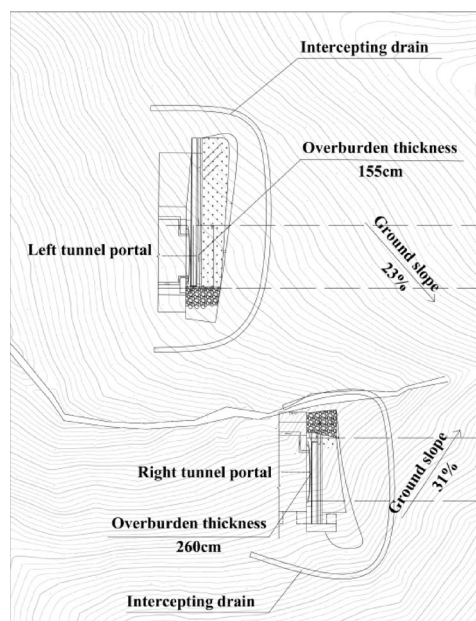


Fig. 1. Schematic plan view of left and right tunnel portal sections.

regression function analysis. The principal innovations of this work are as follows: (1) revealing the evolution of tunnel stability during single-side drift method construction by coupling the deformation behavior of weathered slate with the mechanical response of the support system; (2) introducing the BiDoseResp function model to achieve high-precision fitting and prediction of multi-stage settlement in shallow-buried tunnels under large asymmetrical pressure; and (3) proposing an excavation sequence optimization and risk control strategy based on simulation analysis of the left portal section. The findings are expected to furnish theoretical support and technical guidance for the design optimization and construction safety of similar tunnel projects.

Engineering background

The tunnel investigated in this study is a separated twin-tunnel located in Qinghai Province, with left and right lines each exceeding 600 m in length, classifying it as a medium-sized tunnel. The maximum burial depth reaches approximately 125 m. In contrast, the portal sections of both lines are significantly shallower: the right portal has an overburden thickness of only 1.8 m under a ground slope of 27°, while the left portal exhibits an overburden of merely 1.5 m with a ground slope of 25°. These portal sections are characterized as shallow-buried tunnels under large asymmetrical pressure. For the Class V shallow-buried soft rock encountered at the portals, the corresponding support measures are summarized in the Table 1 below.

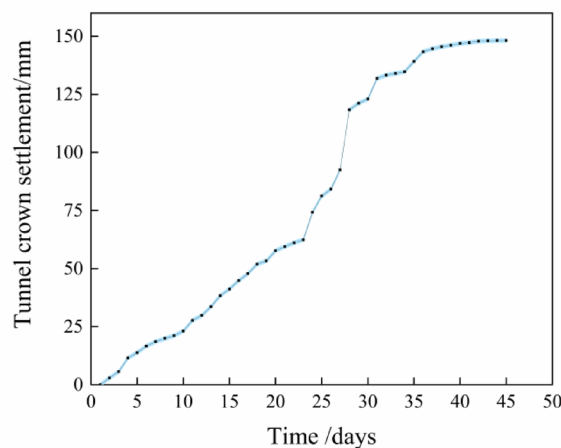
The underground excavation and portal sections of the tunnel are characterized by shallow burial depth and significant asymmetrical pressure. The surrounding rock at the entrance and exit sections consists primarily of moderately to highly weathered slate from the Middle Triassic Series. The overlying surface layer comprises meadow soil and silty deposits, which exhibit low strength and poor stability. The soil is generally loose, rock strata are fractured, and the rock mass is fragmented to relatively fragmented. These geotechnical conditions contribute to poor slope stability, predisposing the area to small-scale collapses and consequently elevating construction risks. Shortly after the underground excavation commenced at the right tunnel portal, issues such as excessive vault settlement and surface cracking were observed. A planar schematic diagram of the portal section is provided in Fig. 1.

Monitoring and analysis of construction anomalies

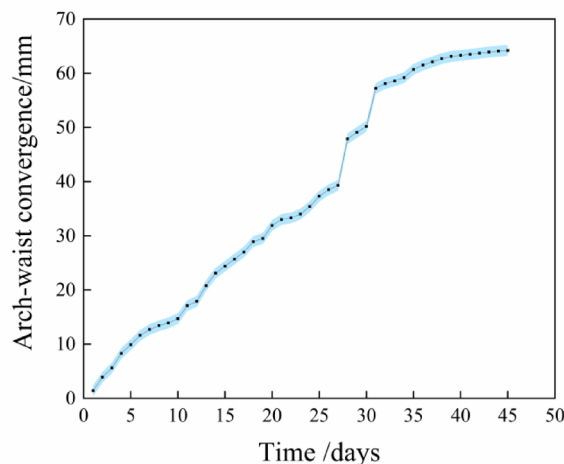
Following the commencement of excavation at the right tunnel portal, pronounced subsidence of the tunnel vault was recorded on the 28th day, accompanied by the development of multiple surface cracks, thereby reaching a red-alert status. Figure 2 illustrates the settlement curve obtained from monitoring point GD01, located at the uppermost section of the tunnel crown in the right portal area, together with the horizontal convergence curve measured at point SL01, positioned at mid-height on the sidewalls. Data points represent mean values, and error bars denote ± 1 standard deviation ($n=3$).

Analysis of the monitoring data yields the following observations:

- (1) Following tunnel excavation, vault settlement at the portal section displayed a continuously increasing trend with time. The maximum settlement value of 14.8 cm was recorded at measurement point GD01, located at the upper left crown of the right portal. Settlement rates at both monitoring points increased rapidly in a nearly linear pattern, with a pronounced inflection point identified. The temporal coincidence of this inflection point with the removal of the central partition wall indicates that this operation served as the critical trigger for the accelerated vault settlement.
- (2) After excavation, the peripheral convergence within the portal section also exhibited a continuously growing trend. The maximum horizontal convergence value exceeded 6 cm at measurement point SL01 at the arch waist of the right portal section, with its rate of change continuing to increase rapidly and showing a distinct inflection point. Chronologically, this inflection point aligns with that observed in the vault settlement rate.



(a)



(b)

Fig. 2. Monitoring data from settlement observation points at the right tunnel portal. (a) Tunnel crown settlement (b) Tunnel arch waist convergence.

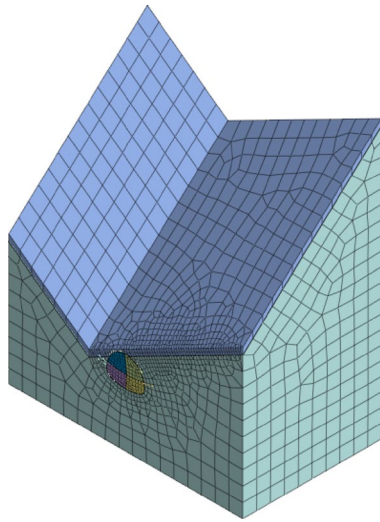


Fig. 3. Three-dimensional numerical model of the right tunnel portal section.

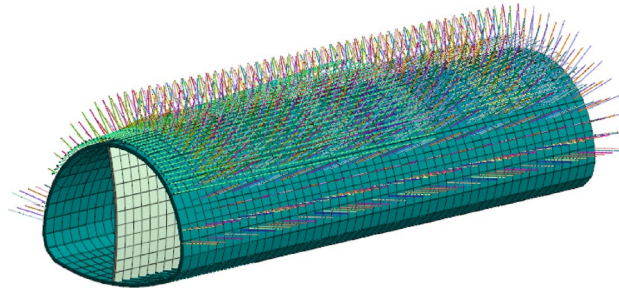


Fig. 4. Schematic diagram of the support structure model.

Longitudinal cracks have developed on the tunnel surface. Together with transverse cracks oriented along the tunnel axis, these fractures roughly delineate a potential landslide mass above the tunnel. This crack pattern indicates that both the tunnel structure and surrounding rock have reached a state of high instability.

Numerical simulation analysis of the shallow-buried and heavily biased section at the right tunnel portal

Model establishment

A three-dimensional finite element model of the shallow-buried, large asymmetrical pressure section at the right tunnel portal was established using specialized geotechnical analysis software. The model extends 84.4 m horizontally, up to 100 m vertically, and 50 m longitudinally along the tunnel axis. The ground surface inclination and stratigraphic divisions were derived from the engineering topographic map and geological longitudinal profile. The detailed configuration of the three-dimensional finite element model is presented in Fig. 3.

The numerical model incorporates support measures—including large pipe roofs, advanced small ducts, systematic rock bolts, primary support, steel arches, and internal partition walls—simulated in accordance with the actual construction sequence. The dimensions of all supporting elements were strictly determined based on the construction drawings. Figure 4 provides a schematic diagram of the three-dimensional finite element model for the support system. In terms of boundary conditions, the ground surface is treated as a free boundary, the model base is vertically constrained, and the front, back, left, and right lateral boundaries are assigned normal constraints.

Parameter selection

In the three-dimensional model, the primary support and internal partition walls were simulated using two-dimensional shell elements. Pipe roofs, advanced small conduits, and rock bolts were modeled with one-dimensional embedded truss elements, whereas steel arches were represented by one-dimensional beam elements. According to geological survey data, the portal section passes through successive layers of slope-deposited silt and strongly weathered Triassic slate, both of which were discretized using three-dimensional solid elements. The corresponding numerical parameters were selected based on the geological investigation report and the *Engineering Geology Handbook*²⁷. All parameters were determined through comprehensive analysis of field

| Material | Unit weight (kN/m ³) | Elastic modulus(MPa) | Poisson's ratio | Cohesion (kPa) | Friction angle (°) |
|--------------------------|----------------------------------|----------------------|-----------------|----------------|--------------------|
| Silty soil | 22 | 13 | 0.3 | 11 | 36 |
| Strongly weathered slate | 21.5 | 22 | 0.16 | 31 | 29 |
| Shotcrete | 25 | 29 | 0.3 | – | – |
| Steel | 78.5 | 200 | 0.3 | – | – |

Table 2. Mechanical property parameters of materials.

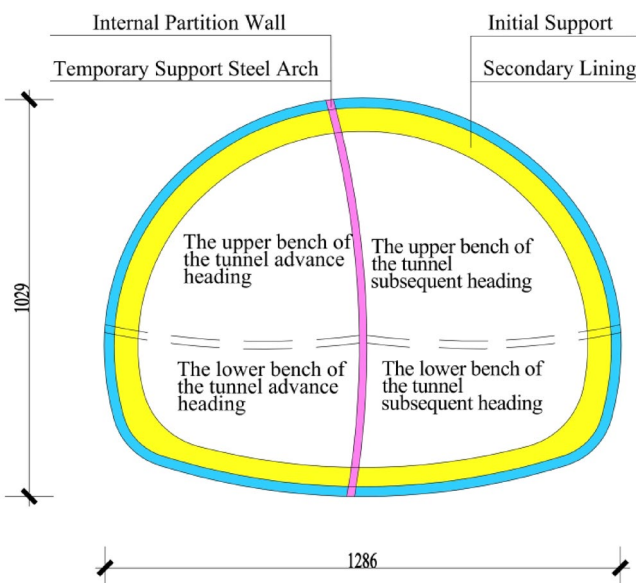


Fig. 5. Tunnel construction layout (unit: cm).

geological surveys and laboratory tests, ensuring both regional representativeness and engineering applicability. The specific physical and mechanical parameters are summarized in Table 2.

This study employed the Drucker-Prager (D-P) yield criterion to simulate the plastic behavior of the surrounding rock. The D-P criterion provides superior numerical stability in three-dimensional finite element analyses and is well-suited for capturing the nonlinear response and stress redistribution of rock masses under asymmetric loading conditions. In contrast to the Mohr–Coulomb criterion, the smooth yield surface of the D-P model promotes improved convergence in numerical simulations, making it particularly appropriate for modeling scenarios involving abrupt stiffness variations, such as the removal of the middle partition wall. Previous research has also demonstrated the effectiveness of the D-P criterion in simulating geomechanical interactions, especially for investigating macroscopic rock failure mechanisms²⁸. For instance, Karakus & Fowell²⁹ adopted the D-P model to ensure computational stability in their analysis of settlement induced by tunnel excavation. The numerical model incorporated the following boundary conditions: the ground surface was treated as a free boundary, the base was fixed in the vertical direction, and the lateral boundaries (front, back, left, and right) were constrained along their respective normal directions. To account for the influence of groundwater and surface loading, an initial groundwater level was defined. Below this level, geotechnical materials were assigned submerged unit weights to simulate their effective stress state under hydrostatic conditions, with pore water pressures automatically computed and applied by the software. Additionally, a uniformly distributed load of 20 kPa was applied across the ground surface to simulate potential vehicle traffic and construction activities.

Construction process simulation

The right tunnel portal passes through a Grade V surrounding rock section characterized by shallow burial depth and significant asymmetrical pressure in soft rock and soil. In accordance with the design specifications, excavation is carried out using the single-side drift method. The side pilot tunnel is divided into upper and lower benches with a total length of 5 m. The advance pilot tunnel and the subsequent main tunnel excavation are staggered by at least 20 m, with each excavation cycle limited to 0.5–1.0 m. Primary support is installed immediately after each excavation step. A schematic of the tunnel construction layout is provided in Fig. 5. The construction sequence is implemented as follows: First, the upper bench of the advance pilot tunnel is excavated, followed by immediate installation of the primary support. Subsequently, the lower bench of the advance pilot tunnel is excavated and similarly supported. Next, the upper bench of the succeeding tunnel section is excavated and primarily supported, after which the lower bench, including the tunnel invert, is excavated and supported.

The process concludes with the removal of temporary supports and the construction of the final lining for both the invert and the arch-sidewall regions.

In the three-dimensional numerical model of the right portal section, the solid mesh is partitioned into blocks corresponding to the actual construction stages of the single-side drift method. These blocks are further subdivided according to the excavation advance length to ensure consistency between the simulated excavation face dimensions and the actual construction parameters. During the definition of construction stages in the model, the blocks are systematically activated and deactivated according to the actual construction sequence, thereby accurately replicating the real excavation process. The schematic diagram of the mesh generation for the specific tunnel excavation model is presented in Fig. 6.

Comparative analysis of calculated results and actual monitoring data for the right tunnel portal

Analysis of results

During the excavation simulation performed with computational analysis software, examining the variation patterns in displacement contours of the tunnel structure can reveal the influence characteristics of excavation on the portal section of shallow-buried tunnels under large asymmetrical pressure. A three-dimensional model of the right portal section—representing shallow burial under significant asymmetrical loading—was simulated following the actual excavation sequence, yielding displacement contour results under various construction phases. Among these, the displacement contours after final tunnel excavation without temporary support removal (i.e., with the middle partition wall retained) and those after temporary support removal are presented in Fig. 7. The simulated trend of tunnel vault settlement is shown in Fig. 8. According to the simulation results, vault settlement increases progressively with excavation advance. The most pronounced increase—reaching 32%—occurs during the removal of the middle partition wall. The settlement eventually stabilizes at a final value of 14.12 cm.

Analysis of the displacement contours yields the following excavation response characteristics for shallow-buried tunnels under large asymmetrical pressure:

- (1) Asymmetrical Pressure Effect: The uneven overburden thickness on either side of the tunnel—thin soil cover on the shallow-buried side and thicker cover on the deep-buried side—results in a concentration of surrounding rock pressure toward the deep-buried side. As a consequence, the shallow-buried side is susceptible to free-face instability and excessive vault settlement.
- (2) Shallow-Buried Risk: In cases of insufficient overburden thickness, the excavation face is prone to breaking through to the ground surface, potentially leading to collapse. The surrounding rock on the shallow-buried side exhibits poor self-stabilization capacity and is highly sensitive to excavation-induced disturbances.

Comparative analysis of actual monitoring and measurement data

In accordance with Article 6.43 of the *Technical Specification for Monitoring and Measurement in Highway Engineering* (DB45/T 1958–2019), the allowable limit for vault settlement in this project is specified as 0.16 m³⁰. Field monitoring data indicate that the settlement observed during actual construction remains within this stipulated threshold, thereby confirming compliance with the relevant regulatory requirements.

Based on the results obtained from the three-dimensional numerical model of the shallow-buried, large asymmetrical pressure section at the right tunnel portal, the maximum displacement during excavation and support occurs at the crown of the upper bench of the pilot tunnel, with a simulated value of 14.12 cm. The corresponding field monitoring data recorded a value of 14.82 cm, resulting in a discrepancy of less than 5%. Figure 9 presents the comparative results of vault settlement deformation at the right tunnel portal. This close agreement validates the reasonableness and reliability of the model parameters. Consequently, the simulation results can be effectively referenced to inform and guide actual construction operations.

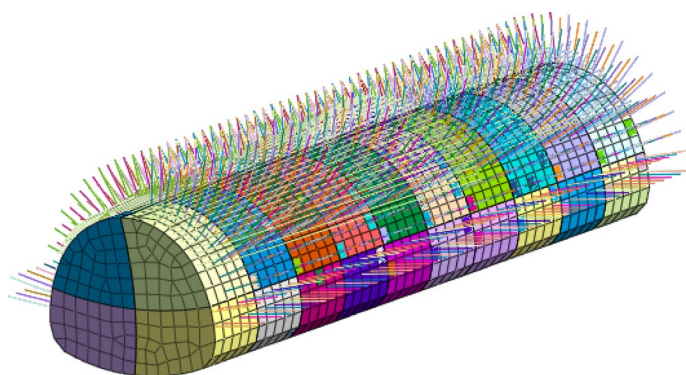
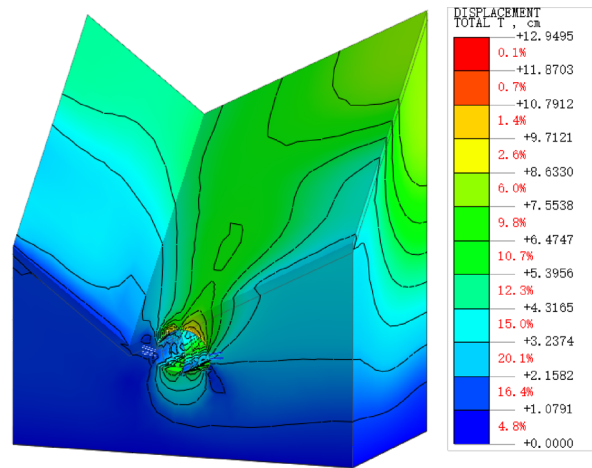
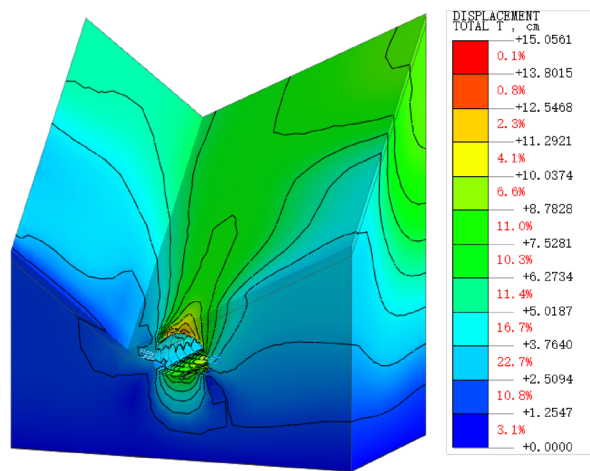


Fig. 6. Mesh generation for tunnel excavation.



(a)



(b)

Fig. 7. Displacement contours of the numerical model. (a) Model diagram of excavation completion without removing the middle partition wall (b) Model diagram of excavation completion with the middle partition wall removed.

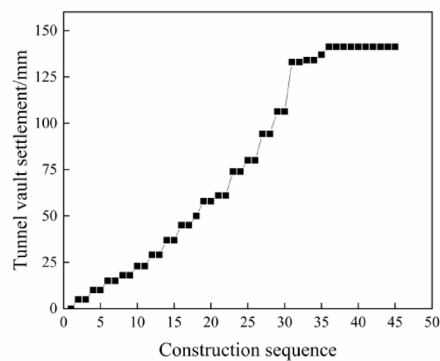


Fig. 8. Simulated trend of tunnel vault settlement calculation.

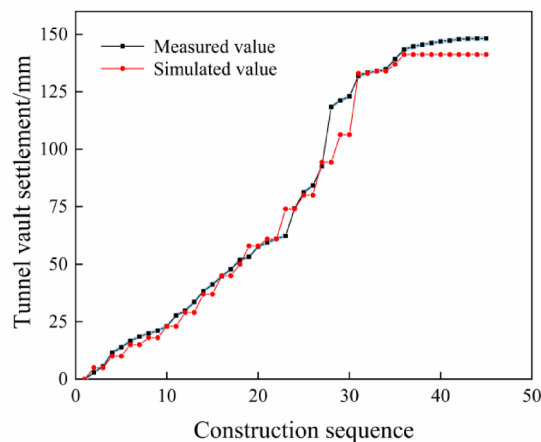


Fig. 9. Comparison of vault settlement deformation at the right tunnel portal.

Quantitative analysis of the “triple effects” induced by middle partition wall removal

To thoroughly investigate the impact of the critical procedure of middle partition wall removal on surrounding rock stability during the construction using the single-side drift method, this section conducts a quantitative analysis of the “Triple Effects”—namely, stress redistribution, soil unloading, and abrupt change in support stiffness—based on a validated numerical model.

Stress redistribution effect

Figure 10 presents contour plots of the maximum principal stress in the surrounding rock before and after removal of the middle partition wall. Before removal, the middle partition wall acted as the main load-bearing member, effectively transferring the higher asymmetrical pressure from the deep-buried side to the foundation (Fig. 10a). Following its removal, the original load path was disrupted, causing stress to be rapidly redistributed to the primary support. Quantitative analysis shows that the maximum principal stress at the tunnel invert increased by 20.36 kPa, while stress concentrations intensified notably in the arch waist and sidewall footing regions, with a maximum stress increase of 39.41 kPa. These results clearly demonstrate a “jump-transfer” mechanism, whereby the load originally carried by the temporary support (middle partition wall) is abruptly shifted to the permanent primary support system.

Soil unloading and plastic zone development

The removal of the middle partition wall effectively eliminates lateral constraint on the surrounding rock, thereby inducing significant unloading and rebound. As illustrated in the plastic strain contour plots of Fig. 11, this process resulted in a notable expansion of the plastic zone around the shoulder and arch foot on the deeply buried side, extending approximately 3.09 m further into the surrounding rock. Within this region, the average plastic strain increased markedly from 1.7×10^{-3} prior to removal to 2.8×10^{-3} afterward. This pronounced increase confirms that the unloading process promoted the propagation and interconnection of internal fractures within the rock mass, representing the fundamental mechanism driving the rapid deformation observed.

Abrupt change in support stiffness effect

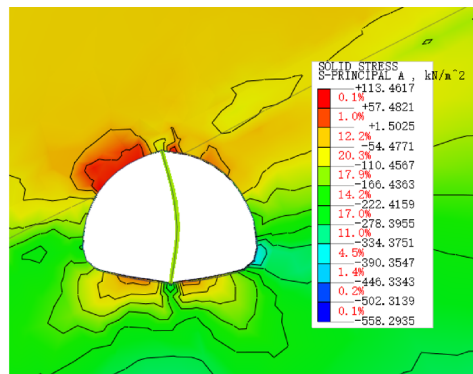
The presence of the middle partition wall significantly enhanced the overall stiffness of the support system. Its removal directly resulted in a reduction of the system’s global stiffness. Analysis of the internal forces in the primary support revealed that, following the removal, the bending moment at the tunnel crown increased instantaneously by 60.4%, and the axial force increased by 41.1%. These values quantify the process whereby the support structure is forced to bear additional loads due to the abrupt stiffness change, explaining the increased risk of failure in the remaining support structure after this procedure.

Interaction mechanism and evolutionary path

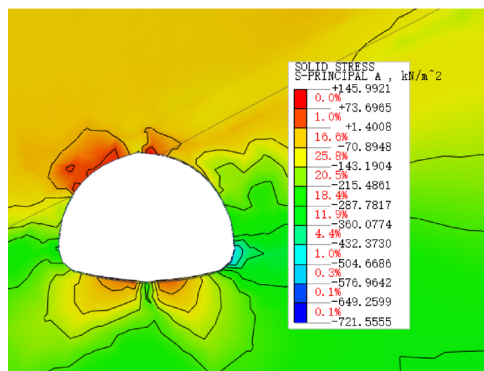
Based on the quantitative analyses above, the interaction mechanism of the “Triple Effects” is clarified: stress redistribution acts as the trigger, altering the stress state of the surrounding rock; soil unloading is the response, manifested as the expansion of the plastic zone and a sharp increase in deformation; and the abrupt change in support stiffness acts as an amplifier, compelling the remaining support structure to bear the additional loads induced by both redistribution and unloading under reduced stiffness conditions. The coupling of these three effects ultimately leads to a step-like increase in crown settlement.

Comparative study of regression analysis functions

Existing studies have established that tunnel vault settlement evolves temporally with distinct patterns. To precisely analyze these deformation characteristics and minimize the influence of extraneous factors, researchers



(a)



(b)

Fig. 10. Maximum principal stress contours of the numerical model. (a) Maximum principal stress nephogram before removal (b) Maximum principal stress nephogram after removal.

commonly perform regression analysis on monitoring data using functions such as exponential and hyperbolic models³¹. Nevertheless, when applied to the portal section of the shallow-buried tunnel under large asymmetrical pressure in this study, these conventional functions failed to produce satisfactory fitting results.

To address this limitation, the BiDoseResp function model was identified as a promising alternative. Distinguished by its capacity to accurately represent dual-dose response relationships, this model demonstrates strong applicability in simulating and analyzing the settlement behavior of shallow-buried tunnels under large asymmetrical pressure. It effectively integrates the complex influences of multiple factors—such as geological conditions and construction procedures—on settlement development, while mathematically capturing the inherent nonlinearity of these interactions. The expression of the BiDoseResp function model is given as follows:

$$y = A1 + (A2 - A1) \left[\frac{P}{1 + 10^{(LOGx01-x) \times h1}} + \frac{1 - P}{1 + 10^{(LOGx02-x) \times h2}} \right] \quad (1)$$

where y denotes the vault settlement (mm), x represents the time variable (days), and $A1$, $A2$, P , $h1$, and $h2$ are fitting parameters.

Although the BiDoseResp function originates from the double-dose response model in pharmacology, its mathematical structure of a biphasic response can effectively describe the key mechanical processes during the construction of shallow-buried tunnels under significant asymmetric pressure using the single-side drift method. This provides the model with clear physical significance in the present study:

Parameters $A1$ and $A2$: Represent the initial settlement value and the final stabilized settlement value, respectively. Their difference ($A2 - A1$) reflects the total settlement induced by tunnel excavation and the subsequent removal of the middle partition wall.

Parameters $LOGx01$ and $h1$: Jointly define the first settlement phase, corresponding to the “excavation disturbance phase.” This stage is primarily governed by stress redistribution and initial plastic deformation caused by the sequential excavation of tunnel sections. Here, $LOGx01$ denotes the time node of this phase, while $h1$ represents the response rate coefficient of the first phase.

Parameters $LOGx02$ and $h2$: Jointly define the second settlement phase, corresponding to the “creep phase after middle partition wall removal.” This phase clearly captures the phenomenon wherein the removal of the temporary support (middle partition wall) leads to an abrupt change in the stiffness of the support system,

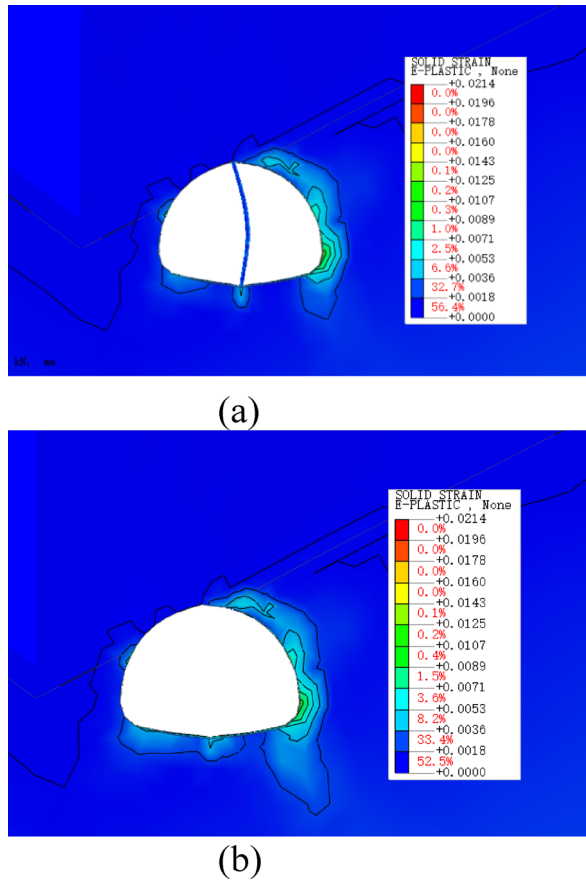


Fig. 11. Equivalent plastic strain contours of the numerical model. (a) Effective plastic strain nephogram before removal. (b) Effective plastic strain nephogram after removal.

| | Value | Standard error |
|--------|-----------|----------------|
| A1 | -27.34168 | 16.00571 |
| A2 | 155.22681 | 5.35886 |
| LOGx01 | 13.47593 | 3.52308 |
| LOGx02 | 27.65859 | 0.29199 |
| h1 | 0.04204 | 0.00792 |
| h2 | 0.24903 | 0.04891 |
| p | 0.69619 | 0.0579 |

Table 3. BiDoseResp function parameter calculation results.

resulting in rapid stress adjustment and accelerated deformation of the surrounding rock. *LOGx02* indicates the time node of this phase, and *h2* is the response rate coefficient of the second phase—the larger its value, the faster the settlement rate.

Parameter *P*: Represents the contribution proportion of the first settlement phase (excavation disturbance) to the total settlement potential ($A2 - A1$), whereas $(1 - P)$ represents the contribution proportion of the second phase (middle partition wall removal).

Thus, the BiDoseResp model utilized in this study functions as a hybrid mechanism-data model that quantitatively characterizes the coupled mechanical process of “excavation disturbance—temporary support removal.” It accurately captures the nonlinear deformation behavior of shallow-buried tunnels under asymmetrical pressure during multi-stage construction. The high goodness-of-fit (R^2) further validates the applicability of this dual-phase mechanical hypothesis under such tunneling conditions.

The vault settlement monitoring data were processed through the model using the Levenberg-Marquardt optimization algorithm for parameter iteration. The resulting parameters for the nonlinear regression curve are listed Table 3 below:

Summarizing the calculated parameters, the BiDoseResp function fitting formula is obtained as:

| F-statistic | Numerator degrees of freedom | Denominator degrees of freedom (DF) | Probability > F (P-value) |
|-------------|------------------------------|-------------------------------------|---------------------------|
| 10.24019 | 7 | 76 | 5.72835E-9 |

Table 4. F-test statistics.

| No. | Function model | RMSE (mm) | Coefficient of determination (COD, R ²) |
|-----|----------------|-----------|---|
| 1 | BiDoseResp | 0.43 | 0.99567 |
| 2 | Logistic | 1.57 | 0.97834 |
| 3 | Boltzmann | 0.81 | 0.98457 |
| 4 | Allometrie1 | 1.76 | 0.96017 |
| 5 | Voigt | 0.78 | 0.98882 |
| 6 | ExpAssoc | 1.83 | 0.95773 |
| 7 | BiHill | 1.73 | 0.96534 |
| 8 | SGompertz | 1.59 | 0.9764 |

Table 5. Comparison of function model fittings.

$$y = -27.34168 + (155.22681 + 27.34168) \left[\frac{0.69619}{1 + 10^{(13.47593-x) \times 0.04204}} + \frac{1 - 0.69619}{1 + 10^{(27.65859-x) \times 0.24903}} \right] \quad (2)$$

The coefficient of determination (R²) for this fitting formula is 0.99567256547728. This high degree of fit indicates that the BiDoseResp function model closely aligns with the actual monitoring data and is highly suitable for analysis in this engineering project.

To enhance the validation of the three-dimensional numerical simulation model's predictive capabilities, the tunnel vault settlement results obtained from numerical simulation were compared with the BiDoseResp function model, and an F-test was conducted. The F-test results are shown in the following Table 4:

The calculated F-statistic is 10.24019, with a corresponding p-value of 5.72835×10^{-9} . This result indicates that the numerical simulation data of tunnel vault settlement exhibit a probability of 99.999999427165% ($1 - 5.72835 \times 10^{-9}$) of being appropriately described by the BiDoseResp model. Such an exceptionally high consistency demonstrates a remarkable agreement between the simulated settlement behavior and the model's functional representation.

Furthermore, comparative analyses with other functional models were performed, as detailed in the Table 5 below. The BiDoseResp model, with its two-stage response mechanism, effectively captures the coupled effects of excavation disturbance and surrounding rock creep. This representation aligns well with the abrupt deformation characteristics observed before and after removal of the middle partition wall. Additionally, the model distinctly characterizes the differential evolution of vault settlement during the early, intermediate, and late phases of the single-side drift excavation process. In contrast, conventional exponential models are limited to representing the influence of a single factor. A comprehensive comparison confirms that the BiDoseResp model provides the most accurate representation of vault settlement behavior in shallow-buried tunnels under large asymmetrical pressure excavated by the single-side drift method.

In summary, integrating field monitoring data with numerical simulation results reveals that the removal of the middle partition wall induces a triple-effect mechanism comprising stress redistribution, soil unloading, and abrupt support stiffness reduction. This study is the first to quantitatively characterize the spatiotemporal coupling behavior of this process using the BiDoseResp function, demonstrating its high applicability and predictive accuracy for settlement analysis in shallow-buried tunnels under large asymmetrical pressure. The model provides an effective approach for fitting tunnel settlement curves with improved reliability. Furthermore, the close agreement between simulation results and monitoring data confirms the reasonableness of the numerical model and parameters adopted for the right tunnel. Accordingly, the same modeling strategy can be applied to simulate the shallow-buried asymmetrical pressure section of the left tunnel portal, supporting further comparative analysis and construction guidance.

Analysis of excavation sequence for the shallow-buried large unsymmetrical pressure section of the left portal Introduction to the construction model

The three-dimensional geotechnical finite element analysis software employed for the left tunnel portal's shallow-buried section under significant asymmetrical pressure is identical to that used for the right portal section. The model extends 84.4 m horizontally, up to 90.4 m vertically, and 50 m longitudinally. Surface inclination and stratigraphic division were derived from the engineering topographic map and geological profile, with a schematic illustration provided in Fig. 12. The initial stress field applied in the simulation matches that utilized in the right portal analysis.

The numerical model for the left tunnel portal section incorporates support measures—including large pipe roofs, advanced small conduits, systematic rock bolts, primary support, steel arches, and internal partition walls—simulated in accordance with the actual construction sequence. All support element dimensions were strictly

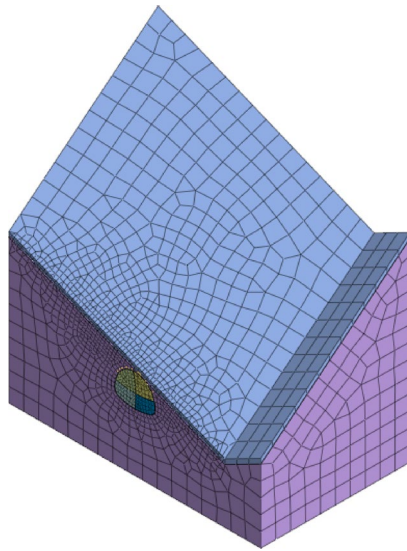


Fig. 12. Three-dimensional numerical model of the left tunnel portal section.

determined based on construction drawings. Boundary conditions and material parameters were consistently adopted from the validated three-dimensional finite element model of the right tunnel portal. Tunnel excavation follows the single-side drift method, with specific procedures aligned with those implemented in the right tunnel simulation, ensuring both models reflect the same actual construction process.

Study on excavation sequence of the single-side drift method for shallow-buried large unsymmetrical pressure tunnels

Using the established three-dimensional numerical model, this study systematically investigates the influence mechanisms of single-side drift method construction procedures on the structural response of shallow-buried tunnels under large asymmetrical pressure. Particular emphasis was placed on comparing the evolution patterns of vault displacement, axial force, and bending moment under two distinct excavation sequences: Scheme A, initiating excavation from the shallow-buried side upper bench pilot tunnel, and Scheme B, commencing from the deep-buried side upper bench pilot tunnel. The principal findings are summarized as follows:

Analysis of bending moment response

Comparison of vault bending moment contours (Fig. 13a,b) reveals that under Scheme A, bending moments at the left and right vaults reach 1.04 and 1.58 times those under Scheme B, respectively. Monitoring data for the middle partition wall (Fig. 13c) indicate that the maximum bending moment in Scheme B exceeds that in Scheme A by 5.31%, yet remains within the safe threshold. Overall, Scheme B demonstrates superior control over vault bending moments, though enhanced stress monitoring of the middle partition wall is recommended during its implementation.

Characteristics of axial force distribution

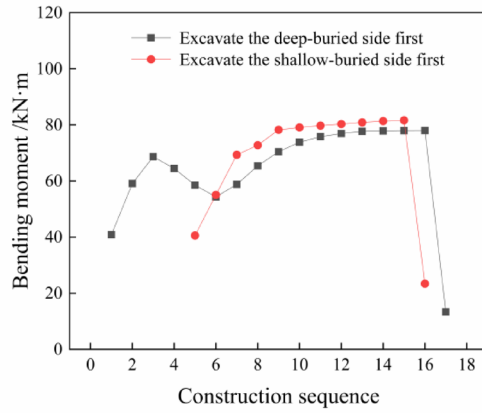
As shown in Fig. 14, axial forces in the left vault, right vault, and middle partition wall under Scheme A are 55.9%, 42.6%, and 374.1% higher, respectively, than those under Scheme B. Excavating the deep-buried side first effectively alleviates structural axial compression, confirming that Scheme B offers significantly better axial force control than Scheme A.

Displacement control efficiency

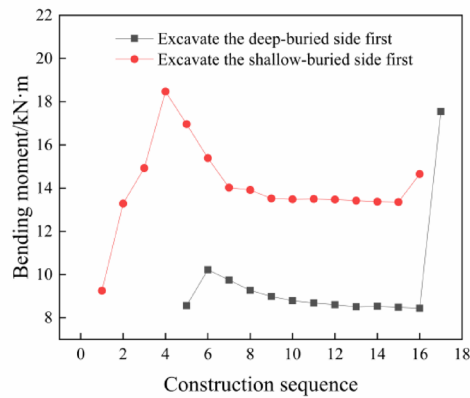
Displacement monitoring curves (Fig. 15) illustrate that under Scheme A, settlement on the deep-buried side (left vault) is 16.2%–17.7% lower than under Scheme B. During the period from stable excavation to middle partition wall removal, settlement values for the two schemes are close, with Scheme A even exceeding Scheme B by 0.4%. In contrast, during the construction phase, shallow-buried side (right vault) settlement under Scheme B is 18.4%–20.5% lower than under Scheme A, and remains 2.5%–6.3% lower during the stable-to-wall-removal stage. Considering the higher collapse risk on the shallow-buried side, Scheme B is more advantageous in controlling displacement during critical construction stages. It is advised to strengthen real-time monitoring of the deep-buried side vault when adopting this scheme.

Comprehensive mechanical response and risk assessment

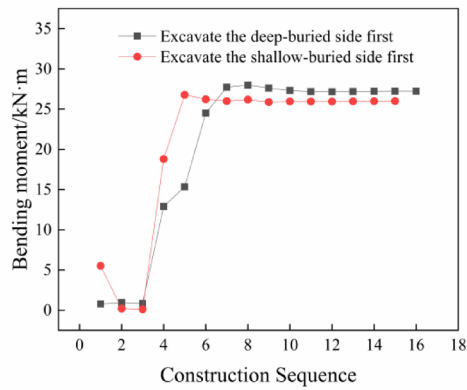
A comprehensive evaluation of bending moments, axial forces, and displacements indicates that the primary risk in this shallow-buried tunnel under asymmetrical pressure originates from the high surrounding rock pressure on the deep-buried side. Adopting a construction sequence that begins with excavating the deep-buried side and promptly installing supports (including the middle partition wall) enables the formation of a “rigid



(a)



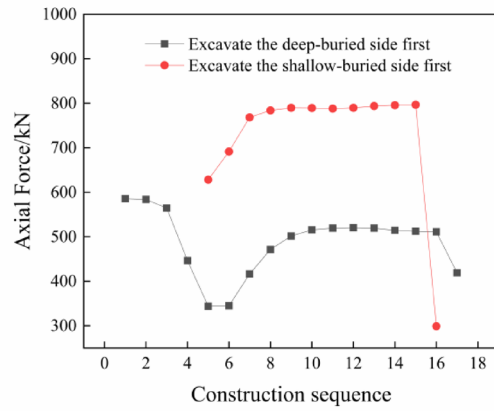
(b)



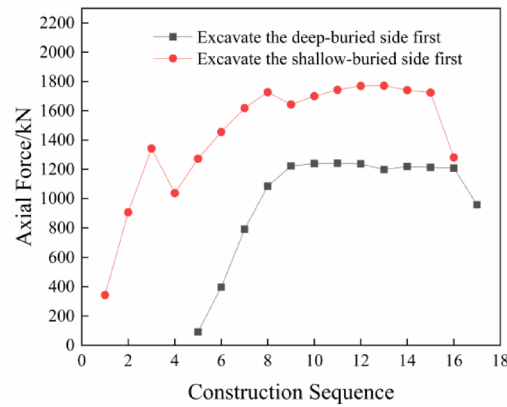
(c)

Fig. 13. Comparison of bending moment values at monitoring points. (a) Comparison diagram of left vault monitoring points. (b) Comparison diagram of right vault monitoring points (c) Comparison diagram of central diaphragm monitoring points.

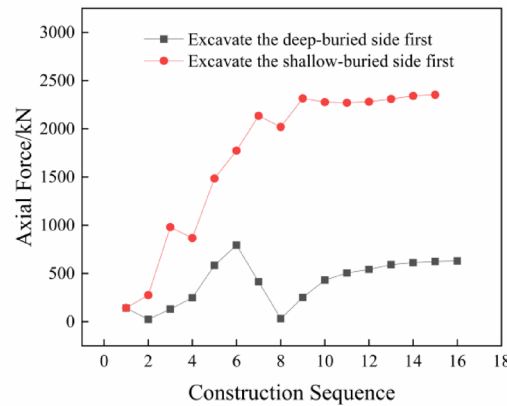
support system.” This system restrains the surrounding rock on the deep-buried side from intruding into the tunnel space, thereby mitigating adverse effects on the shallow-buried side. During subsequent excavation of the shallow-buried side, the pre-established supports on the deep-buried side, together with the middle partition wall, act as temporary stabilization measures. This configuration reduces the effective span of the excavation face



(a)

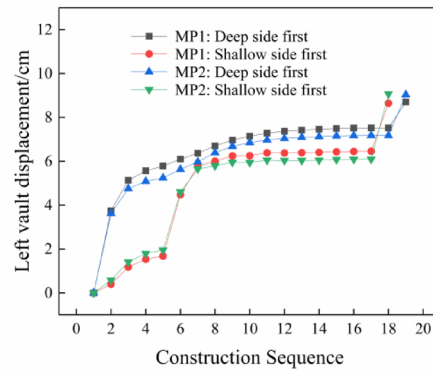


(b)

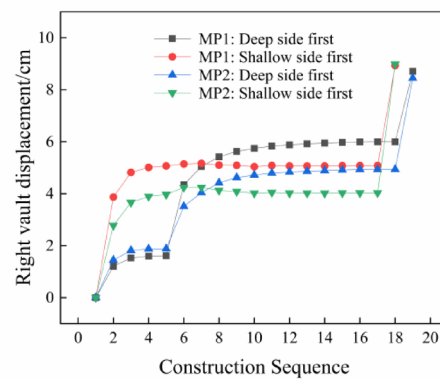


(c)

Fig. 14. Comparison of axial force values at monitoring points (a) Comparison diagram of left vault monitoring points (b) Comparison diagram of right vault monitoring points (c) Comparison diagram of central diaphragm monitoring points.



(a)



(b)

Fig. 15. Comparison of settlement values at monitoring points (a) Settlement comparison diagram of left vault monitoring points (b) Settlement comparison diagram of right vault monitoring points.

and facilitates rapid support installation after excavation. Ultimately, the integration of supports from both sides forms a closed load-bearing structure, significantly enhancing the overall resistance to asymmetrical pressure.

Time and cost benefits of excavation sequence optimization

While this study primarily addresses the mechanical behavior associated with excavation sequences, the potential benefits of Scheme B (deep-buried side first) in terms of project duration and cost merit consideration. From a process standpoint, Schemes A and B involve identical numbers and complexities of construction steps; they differ only in the lateral excavation sequence. Consequently, Scheme B does not introduce additional procedures or substantially extend individual cycle durations.

Its principal advantages in schedule and cost derive from risk reduction. As demonstrated in earlier analyses, Scheme A (shallow-buried side first) led to a maximum increase of 55.9% in axial support force and 18.4%–20.5% greater vault settlement, significantly elevating the risks of support failure, surrounding rock instability, and potential local collapse. Should such scenarios occur, subsequent remediation—such as work suspension, additional reinforcement, and emergency stabilization—would incur unforeseen delays and cost overruns far exceeding those implied by the sequence adjustment itself. In contrast, Scheme B establishes a “rigid support” system on the deep-buried side at an early stage, creating a safer and more stable environment for subsequent excavation. This approach substantially lowers the probability of construction risks. Although this preventive strategy may require more meticulous cycle-by-cycle management, it effectively ensures construction continuity and stability, thereby improving the predictability of the project timeline and total investment. Thus, from a life-cycle project perspective, Scheme B offers superior comprehensive benefits.

In summary, for the construction of shallow-buried tunnels under asymmetrical pressure using the single-side drift method, prioritizing excavation of the deep-buried side demonstrates superior effectiveness in mitigating asymmetrical effects and ensuring construction safety. The underlying mechanism involves first addressing the high-pressure side to establish a stable support system before excavating the shallow-buried side, thereby significantly reducing the risk of collapse. As identified in Sect. 5.3, the removal of the middle partition wall

induces a “triple-effect mechanism” that serves as a critical trigger for abrupt settlement. It is therefore essential to strictly control the exposure duration of the middle partition wall during construction. Adherence to the “minimum exposure time” principle helps restrict the development of surrounding rock creep under temporary support conditions, thereby mitigating both initial deformation prior to removal and the potential for sudden settlement increases. To implement this control principle effectively, the middle partition wall should be removed promptly after the primary support strength attains at least 80% of its design value. In principle, the exposure duration should not exceed seven days, subject to dynamic adjustment according to field monitoring data and the creep behavior of the surrounding rock. Concurrently, a “dynamic BiDoseResp prediction” mechanism shall be established, in which vault settlement data are collected every three days and incorporated into the model for rolling prediction and early warning. Should the predicted settlement approach the yellow-alert threshold, construction progress should be timely regulated or local support enhanced, thereby forming a closed-loop risk management system characterized by “monitoring–prediction–adjustment”. Furthermore, the optimal exposure duration should be determined dynamically using field monitoring data—particularly predictions derived from the BiDoseResp model—while maintaining compliance with the required primary support strength. A systematic quantitative investigation of this relationship represents a valuable direction for future research.

Analysis of tunnel vault displacement

Analysis of the recommended scheme indicates that when tunnel excavation is completed but the middle partition wall remains in place, the maximum vault settlement reaches 7.51 cm. Following removal of the middle partition wall, the displacement further increases to 8.7 cm before stabilizing. These values approach or exceed yellow to red alert thresholds under actual construction conditions. The calculated results align with those from the simulation of the right tunnel portal’s shallow-buried section under large asymmetrical pressure, with both exhibiting a characteristic three-stage settlement pattern: an excavation disturbance phase, a middle partition wall removal response phase, and a final lining stabilization phase. In practice, settlement control measures should be implemented specifically for each of these three phases.

Conclusions and suggestions

This study investigated a twin-tunnel project in Qinghai Province characterized by shallow burial depth and large asymmetrical pressure. By integrating field monitoring, numerical simulation, and regression analysis, the research yielded the following findings and recommendations:

- (1) The vault settlement behavior in shallow-buried tunnels under large asymmetrical pressure, excavated using the single-side drift method, closely aligns with the BiDoseResp function model ($R^2 = 0.9957$). The model’s dual-phase response mechanism effectively represents the coupled effects of excavation-induced disturbance and surrounding rock creep. Furthermore, its fitting precision substantially exceeds that of conventional exponential and logistic models, offering an effective alternative for predicting settlement in such tunneling conditions.
- (2) During construction with the single-side drift method, removal of the middle partition wall serves as the critical trigger for abrupt settlement. This process can be quantitatively characterized by a triple-effect mechanism comprising stress redistribution, soil unloading, and abrupt stiffness reduction in the support system. These coupled effects induce a maximum stress increase of 39.41 kPa at the vault, extend the plastic zone approximately 3.09 m into the surrounding rock, and cause marked increases of 60.4% in bending moment and 41.1% in axial force in the support structure, thereby inducing step-like growth in crown settlement.
- (3) Comparative analysis of the two excavation sequences confirms that initiating excavation from the deep-buried side (Scheme B) achieves superior deformation control: it reduces axial forces at the vault by up to 55.9% and decreases settlement on the shallow-buried side by 18.4%–20.5%. By first establishing a rigid support system on the deep-buried side, this method effectively mitigates the adverse effects of asymmetrical loading on the shallow-buried side, lowers the risk of surrounding rock instability during construction, and helps avoid project delays and cost overruns caused by excessive deformation or collapse. Therefore, Scheme B offers enhanced comprehensive engineering benefits.
- (4) Numerical simulation of the left portal section indicates that even with the implementation of Scheme B, the maximum predicted vault settlement reaches 8.7 cm, which remains within the yellow to red alert range. To ensure construction safety, it is essential to rigorously implement a risk control strategy comprising “deep-buried side excavation priority, minimized exposure time of the middle partition wall, and dynamic BiDoseResp-based prediction”.
- (5) Although this study is based on a specific case involving weathered slate in Qinghai, the proposed BiDoseResp-based settlement prediction method, the “deep-buried side first” excavation strategy, and the risk control framework addressing the triple-effect mechanism of middle partition wall removal are fundamentally aimed at managing asymmetrical loading and support stiffness variations. These principles offer valuable references for other weak geomaterials experiencing similar mechanical challenges, such as sandstone and clay. In practical applications, both the model and support design should be adaptively adjusted according to specific mechanical parameters of the target stratum—including cohesion, internal friction angle, and creep characteristics.
- (6) This study did not incorporate a sensitivity analysis of key parameters within the numerical model. Future work should systematically evaluate the influence of parameter variations on simulation outcomes to improve the model’s generalizability and reliability.

Data availability

All data generated or analysed during this study are included in this article.

Received: 2 September 2025; Accepted: 7 November 2025

Published online: 24 December 2025

References

- Wang, K. K. Study on the surface deformation law of tunnel construction in different working procedures by double side heading method. *Railway Constr. Technol.* (6), 113–117. (2020).
- Huang, L. Y. et al. Monitoring and analysis of support structure vibration caused by blasting construction of shallow buried super large section tunnel. *J. Guangxi Univ. Sci. Technol.* **32** (3), 80–85 (2021).
- Pan, J. M. et al. Stability analysis of shallow tunnels subjected to eccentric loads by a boundary element method. *J. Rock Mech. Geotech. Eng.* **8** (4), 480–488 (2016).
- Liu, D. L. Construction scheme and procedure optimization of Large-Section tunnel in shallow and unsymmetrical Pressure. *J. Guilin Univ. Technol.* **32** (1), 77–81 (2012).
- Yang, X. L. & Sui, Z. R. Numerical simulation of construction sequence for shallow embedded bias tunnels with small clear distance. *J. Cent. South. Univ. (Science Technology)*. **38** (4), 764–770 (2007).
- Sharifzadeh, M. et al. Design of sequential excavation method for large span urban tunnels in soft ground-Niayesh tunnel. *Tunn. Undergr. Space Technol.* **35**, 178–188 (2013).
- Li, P. F. & Zhao, Y. Performance of a multi-face tunnel excavated in loess ground based on field monitoring and numerical modeling. *Arab. J. Geosci.* **9** (14), 640 (2016).
- Chen, J. et al. Failure mechanisms and modes of tunnels in monoclinic and Soft-hard interbedded rocks: a case Study. *KSCE J. Civ. Eng.* **24** (4), 1357–1373 (2020).
- Carranza-Torres, C. & Diederichs, M. Mechanical analysis of circular liners with particular reference to composite supports. For example, liners consisting of shotcrete and steel sets. *Tunn. Undergr. Space Technol.* **24** (5), 506 (2009).
- Xiao, J. Z. et al. Analysis of mechanical behavior in a pipe roof during excavation of a shallow bias tunnel in loose deposits. *Environ. Earth Sci.* **75** (4), 293 (2016).
- Das, R. et al. Numerical analysis of surface subsidence in asymmetric parallel highway tunnels. *J. Rock Mech. Geotech. Eng.* **9** (1), 170–179 (2017).
- Tang, J. S., Xiong, B. L. & Liu, C. G. Model test research on excavation method of large-span and shallow-buried bias tunnel in cobble and gravelly soil layer. In *2017 3rd International Forum on Energy, Environment Science and Materials (IFESM 2017)*. 336–343. (Atlantis Press, 2018).
- Wang, K. et al. Deformation failure characteristics of weathered sandstone strata tunnel: A case Study. *Eng. Fail. Anal.* **127**, 105565 (2021).
- Lei, M. F. et al. Model test to investigate the failure mechanisms and lining stress characteristics of shallow buried tunnels under unsymmetrical loading. *Tunn. Undergr. Space Technol.* **46**, 64–75 (2015).
- Lei, M. F. et al. Model test to investigate failure mechanism and loading characteristics of shallow-bias tunnels with small clear distance. *J. Cent. South. Univ.* **23** (12), 3312–3321 (2016).
- Habumuremyi, P. & Xiang, Y. Y. A 3-D analytical continuous upper bound limit analysis for face stability of shallow shield tunneling in undrained clays. *Comput. Geotech.* **164**, 105779 (2023).
- Amiri, S. & Dehghan, A. N. Comparison of shallow tunneling method with pile and rib method for construction of subway station in soft ground. *Front. Struct. Civil Eng.* **16** (6), 704–717 (2022).
- Mojtahedi, A. S., Imani, M. & Fahimifar, A. Three-dimensional face stability analysis of deep and shallow tunnels in rock masses. *Int. J. Geomech.* **21** (10), 040211931–040211920 (2021).
- Zhang, P. et al. Parametric analysis and control of bedding-inclined asymmetric stress in double-arch tunnels: a 3DEC-based study on jointed rock masses. *Buildings* **15** (11), 1816 (2025).
- Chen, H. et al. Study on construction mechanic characteristics and construction optimization of super-large cross-section tunnel portal under shallow buried depth and asymmetrical loading: a case study in Southwest China. *PLOS ONE*. **20** (1), e0316736 (2025).
- Huang, Y., Fang, T. & Wang, N. Excavation method comparison and optimization for a super large cross-section tunnel. *Appl. Sci.* **14** (15), 6544 (2024).
- Feng, T. et al. Failure mechanism and surface settlement analysis of tunnels in an inclined stratum based on the upper bound method. *Tunn. Undergr. Space Technol.* **164**, 106804 (2025).
- Zhao, S., Feng, X. & Peng, K. Prediction and parameter optimization of surface settlement induced by shield tunneling using improved informer algorithm. *Appl. Sci.* **15** (12), 6766 (2025).
- He, J. et al. Investigating the mechanical responses and construction optimization for shallow super-large span tunnels in weathered tuff stratum based on field monitoring and FLAC3D modeling. *Int. J. Civil Eng.* **22** (3), 379–395 (2024).
- Hu, Z. et al. Mechanical behaviors of surrounding rock and supporting structure of shallow-buried unsymmetrical pressure tunnel crossing soil–rock interface. *Front. Earth Sci.* **10**, 1113430 (2023).
- Sun, B. et al. Study on displacement mode and structural failure of jointed surrounding rock of shallow buried tunnel under tectonic stress. *Structures* **70**, 107809 (2024).
- The Editorial Board of "Engineering Geological Handbook". 4th edn (China Architecture & Building Press, 2007).
- Liu, W. et al. Investigation of the tool-rock interaction using Drucker-Prager failure criterion. *J. Petrol. Sci. Eng.* **173**, 269–278 (2019).
- Karakus, M. & Fowell, R. J. Effects of different tunnel face advance excavation on the settlement by FEM. *Tunn. Undergr. Space Technol.* **18** (5), 513–523 (2003).
- Guangxi Zhuang Autonomous Region Department of Transportation. *Technical Regulations for Highway Monitoring Measurement: DB45/T1958-2019* (China Communication Press, 2020).
- Ma, D. et al. Discussion on the timing for the secondary lining construction in soft ground tunnels with high geostress based on numerical simulation and measured data Fitting. *Mod. Tunn. Technol.* **59** (4), 137–146 (2022).

Author contributions

Conceptualization, R.J. Sun, B. Gao; methodology, R.J. Sun, B. Gao, C. Gan; software, C. Gan, J. Zhu; validation, R.J. Sun, B. Gao, D.M. Cai; formal analysis, R.J. Sun, J. Zhu; investigation, R.J. Sun.; resources, B. Gao, D.M. Cai, L.B. Yi; data curation, C. Gan, J. Zhu; writing—original draft preparation, R.J. Sun; writing—review and editing, B. Gao, D.M. Cai; visualization, C. Gan; supervision, B. Gao, L.B. Yi; project administration, B. Gao, L.B. Yi; funding acquisition, B. Gao. All authors have read and agreed to the published version of the manuscript.

Funding

This research was funded by the Natural Science Foundation of Henan Province, China (162102210188); Research and Development Projects of Henan Construction Industry Association (YJX-2023-K01, YJX-2023-K02).

Declarations

Competing interests

The authors declare no competing interests.

Additional information

Correspondence and requests for materials should be addressed to C.G.

Reprints and permissions information is available at www.nature.com/reprints.

Publisher's note Springer Nature remains neutral with regard to jurisdictional claims in published maps and institutional affiliations.

Open Access This article is licensed under a Creative Commons Attribution-NonCommercial-NoDerivatives 4.0 International License, which permits any non-commercial use, sharing, distribution and reproduction in any medium or format, as long as you give appropriate credit to the original author(s) and the source, provide a link to the Creative Commons licence, and indicate if you modified the licensed material. You do not have permission under this licence to share adapted material derived from this article or parts of it. The images or other third party material in this article are included in the article's Creative Commons licence, unless indicated otherwise in a credit line to the material. If material is not included in the article's Creative Commons licence and your intended use is not permitted by statutory regulation or exceeds the permitted use, you will need to obtain permission directly from the copyright holder. To view a copy of this licence, visit <http://creativecommons.org/licenses/by-nc-nd/4.0/>.

© The Author(s) 2025